Sensors & Actuators: B. Chemical 296 (2019) 126616

Contents lists available at ScienceDirect

Sensors and Actuators B: Chemical

journal homepage: www.elsevier.com/locate/snb

# Implementing an artificial synapse and neuron using a Si nanowire ion-sensitive field-effect transistor and indium-gallium-zinc-oxide memristors

Sungju Choi[a], Seohyeon Kim[a], Jungkyu Jang[a], Gumho Ahn[a], Jun Tae Jang[a], Jinsu Yoon[a], Tae Jung Park[b], Byung-Gook Park[c], Dong Myong Kim[a], Sung-Jin Choi[a], Seung Min Lee[a], Eun Young Kim[d], Hyun Sun Mo[a,*], Dae Hwan Kim[a,*]

[a] School of Electrical Engineering, Kookmin University, Seoul 02707, Republic of Korea
[b] Department of Chemistry, Chung-Ang University, Seoul 06974, Republic of Korea
[c] Department of Electrical and Computer Engineering, Seoul National University, Seoul 151-742, Republic of Korea
[d] Department of Biomedical sciences, Ajou University Graduate School of Medicine, Suwon, Kyunggi-do 16499, Republic of Korea

ARTICLE INFO

*Keywords:*
Neuron
Synapse
Silicon nanowire
ISFET
IGZO
Memristor
Brain-inspired computing

ABSTRACT

In this study, we implement an artificial synapse and neuron in a single platform by combining a silicon nanowire (SiNW) ion-sensitive field-effect transistor (ISFET), an indium-gallium-zinc-oxide (IGZO) memristor, and a voltage-controlled oscillator (VCO). The chemical and electrical operations of the synapse are emulated using the pH sensor operation of the ISFET and long-term potentiation/short-term plasticity of the IGZO memristor, respectively. The concentration of hydrogen ions in an electrolyte is successfully transformed via a VCO-based neuron into modulation of synaptic strength, i.e., the current of the memristor. It mimics the strength of the synaptic connection modulated by the concentration of the neurotransmitter. Thus, the chemical-electrical signal conversion in chemical synapses is clearly demonstrated. Furthermore, the proposed artificial platform can discriminate the chemical synapse from the electrical synapse and the path of the neuro-signal propagation and that of memorization/update of synaptic strength. This can potentially provide a new insight into the principles of brain-inspired computing that can overcome the bottleneck of the state-of-the-art von-Neumann computing systems.

## 1. Introduction

Data are currently generated at rates far greater than at which they can be analyzed. Hence, improving the speed and energy efficiency of hardware by orders of magnitude is vital for Internet of Things, telecommunications, and storage systems. However, this is a difficult task when using general hardware based on the complementary metal-oxide-semiconductor (CMOS) technology and von-Neumann architecture since the scaling of the silicon CMOS is approaching its physical limitations [1]. Furthermore, the challenge of the well-known memory wall between the processor and off-chip memory/storage represents the system bottleneck, which negatively affects disk drive input-output rate, process clock speed, and graphics processing unit performance [2].

Researchers have recently started employing brain-inspired neuromorphic computing systems to overcome the limitations of von-Neumann computing systems. Since neural-inspired learning algorithms involve extensive large-scale matrix operations, a computing paradigm that exploits parallelism at fine-grained levels is attractive for overcoming memory walls [3]. The final goal of hardware implementation for brain-inspired computing requires changing the paradigm of conventional hardware for highly demanding application-specific tasks such as image processing, speech recognition, autonomous vehicles, and artificial bodies [4].

Undoubtedly, the emulation of biological systems is an indispensable step toward the design, verification, and implementation of a large-scale integrated neuromorphic system and its architecture. Here, two important concerns should be carefully considered when emulating biological synapses and neurons in the human brain: (1) distinguishing *chemical synapses* from *electrical synapses* and (2) discriminating and implementing the path through which neuro-signals propagate and the path where synaptic strengths are stored and dynamically updated for realizing *plasticity*.

In the case of *chemical synapses*, neurotransmitters from a presynaptic neuron are transferred to a postsynaptic neuron through receptors; the amount of neurotransmitters transferred is converted into

* Corresponding authors.
*E-mail addresses:* tyche@kookmin.ac.kr (H.S. Mo), drlife@kookmin.ac.kr (D.H. Kim).

https://doi.org/10.1016/j.snb.2019.05.093
Received 31 December 2018; Received in revised form 14 April 2019; Accepted 25 May 2019
Available online 08 June 2019

electrical signals, called action potentials, and propagated in the neurons. While there is a time delay in signal transmission owing to this electrical-chemical-electrical signal conversion, signal transmission is unidirectional. Thus, proper chemical function emulation involves detecting the concentration of neurotransmitter agents, i.e., γ-aminobutyric acid (GABA), glycine (inhibitory neurotransmitter), and glutamate (excitatory neurotransmitter) with the functionalization of their specific-binding receptors [5], i.e., the ionotropic glutamate receptor, G-protein coupled receptor, and metabotropic glutamate receptor [6]. On the other hand, in *electrical synapses*, only electrical signals propagate directly from a presynaptic to a postsynaptic neuron through the gap junction channel. Fast and bidirectional signal transmission occurs without involving action potential. Thus, there is no electrical-chemical-electrical signal conversion in electrical synapses [7]. In the nerve system, both the chemical and electrical synapses exist simultaneously and influence each other diversely, as observed in mixed synapses [5].

Meanwhile, in term of *plasticity*, it is noteworthy that the plasticity of synaptic strength occurs simultaneously with the signal propagation. Proper emulation of plasticity involves the long-term potentiation (LTP), short-term plasticity (STP), and spike timing–dependent plasticity (STDP) of the spiking neural network [8]. Moreover, despite the simultaneous chemical and electrical functions of a synapse, they have been studied separately and in an oversimplified manner so far. For instance, the generation and propagation of the action potential and its STDP operation have been demonstrated only by considering the time difference between the presynaptic and postsynaptic pulses with an oversimplified shape that is different from the actual action potential. Furthermore, this disparity makes it difficult to understand how the relationship between the chemical and electrical synaptic functions actually affects the high energy efficiency of the human brain or nervous system because the electrical-chemical-electrical signal transformation in chemical synapse is lacking in such simplified descriptions. More noticeably, although bidirectional signaling is closely related to a very important backpropagation in convolutional neural network; the fact that most studies have demonstrated the synaptic plasticity functions, such as LTP, STP, and Hebbian STDP, without distinguishing between the unidirectional chemical synapse and bidirectional electrical synapse suggests that there is a big gap between the brain nervous system and its emulation.

Therefore, both discriminating the chemical synapse from the electrical synapse and considering signal propagation and memorization/update of synaptic strength separately are essential for the proper systematic implementation of artificial synapses and neurons. In other words, not only the interaction of the chemical and electrical parts of synapses, but also the interactions between the part of signal propagation and the part of memorization/update of synaptic strength should be implemented simultaneously in a single platform to enable studying LTP, STP, and STDP more precisely and in a more realistic manner.

To achieve this end, electrical-chemical-electrical signal conversion in chemical synapses, signal propagation via receptors, and their resultant plasticity of synaptic strength are demonstrated in a single platform by consolidating silicon nanowire (SiNW) ion-sensitive field-effect transistors (ISFETs), amorphous indium-gallium-zinc-oxide (a-IGZO) memristor, and voltage-controlled oscillator (VCO). These results are the steps toward satisfying two abovementioned requirements for implementing artificial synapses and neurons, discriminating a chemical synapse from an electrical synapse, and considering signal propagation and memorization/update of synaptic strength separately.

## 2. Experimental

Fig. 1(a) illustrates the chemical-electrical signal conversion of chemical synapses. During the propagation of neuro-signals through the synapse-neuron-synapse path [A–C in Fig. 1(a)], neurons couple indirectly via the release and diffusion of neurotransmitters. An ejected neurotransmitter is initialized by the action potential of a presynaptic neuron, then diffused from presynaptic neurons to receptors of postsynaptic neurons, and reconverted into action potentials in postsynaptic neurons. Then, the chemical synapse between presynaptic and postsynaptic neurons [A in Fig. 1(a)] corresponds to A in Fig. 1(b) where the SiNW ISFETs, used as bionic chemical synapse circuits, must be sensitive to the concentration of the neurotransmitter to implement a bio-inspired circuit. Indeed, top-down processed SiNW ISFETs have been proposed as promising biosensors because they offer real-time and label-free detection, excellent sensitivity owing to their high surface-to-volume ratio, and compatibility for integration with the conventional complementary metal-oxide-semiconductor (CMOS) technology [9–11].

As shown in Fig. 2(a), the SiNW ISFETs proposed for emulating chemical synapses were fabricated on (100) silicon-on-insulator (top Si layer $=100$ nm and buried oxide $=375$ nm) wafers doped by boron (doping concentration $= 4 \times 10^{15}\,cm^{-3}$). Ion implantation was performed on the Si layer thinned to 80 nm by thermal oxidation to conduct channel doping with a p-type region (dopant: $B^+$, energy: 20 keV, dose: $5 \times 10^{13}\,cm^{-2}$) and n-type region ($P^+$ 40 keV $3 \times 10^{13}\,cm^{-2}$). The annealing process was performed at 950 °C for 30 min to obtain the uniformity of channel doping with the 80-nm-thick silicon channel. Next, the active layer was defined by a combination of electron beam and photolithography (mix-and-match) on the silicon layer. To obtain the active formation and region, the silicon channel layer was etched using $O_2$/HBr inductively coupled plasma (ICP) excitation. Dry-oxidation was performed at 850 °C to form the 10-nm-thick gate oxide and the poly-silicon (thickness $=100$ nm) was deposited at 630 °C using low-pressure chemical vapor deposition (CVD). The poly-silicon on the SiNW was removed using photolithography and ICP dry etching. A photoresist (PR) mask covering only the SiNW channels was then employed to dope the gate (G) and source/drain (S/D) of the SiNW by $As^+$ and $BF_2{}^+$ ion implantation for the n-type and p-type S/D/G, respectively. Rapid thermal annealing was conducted at 900 °C for 10 s to activate the dopants, before the inter-layer dielectric oxide (ILD) was formed using a high-density plasma CVD process. Dry etching and photolithography formed the contact holes. Next, the metal layer (Al) was sputter-deposited and patterned for metallization on the ILD. The tetraethyl orthosilicate layer was then deposited for passivation. Dry etching and photolithography were used to open the pads. To open the sensing area, the oxide layer around the SiNW was removed by photolithography and magnetically enhanced reactive ion etching technique in $CF_4/CHF_3$ plasma. Finally, an alloying process was performed. The SiNW ISFET was fabricated with width $=120$ nm, L

In addition, with regard to synaptic plasticity, most previous studies on the application of memristors as synapses adopted approaches of continuously modulating the memristor conductance according to the time difference of the electrical pulses, i.e., STDP [8,12,13]. The propagation of a neuro-signal through a neuron [B in Fig. 1(a)] corresponds to B in Fig. 1(b), and the plasticity of the synapse [C in Fig. 1(a)] is illustrated in C of Fig. 1(b). In most cases, analog-type resistance-switching (RS) devices with two terminals acted as memristors. On the other hand, a-IGZO memristors enable the effective implementation of electrical synapse devices as they offer the advantages of high mobility, low cost process, large-area uniformity, and compatibility with flexible electronics [14,15].

Therefore, we fabricated the a-IGZO memristor on a p + silicon wafer, as shown in Fig. 2(b). An a-IGZO layer was first deposited on the $p^+$ silicon wafer by radio-frequency (RF) sputtering in an $Ar/O_2$ mixture (3/2 sccm) at room temperature under an RF power of 150 W. Here, the $p^+$ silicon substrate acts as the bottom electrode. The thickness of the IGZO memristor was then optimized to 50 nm. Subsequently, a Pd layer was deposited with an electron-beam evaporator and patterned using a shadow mask to form the 40-nm-thick top electrode.

A top-view scanning electron microscope (SEM) and transmission electron microscope (TEM) images of the fabricated SiNW ISFET are

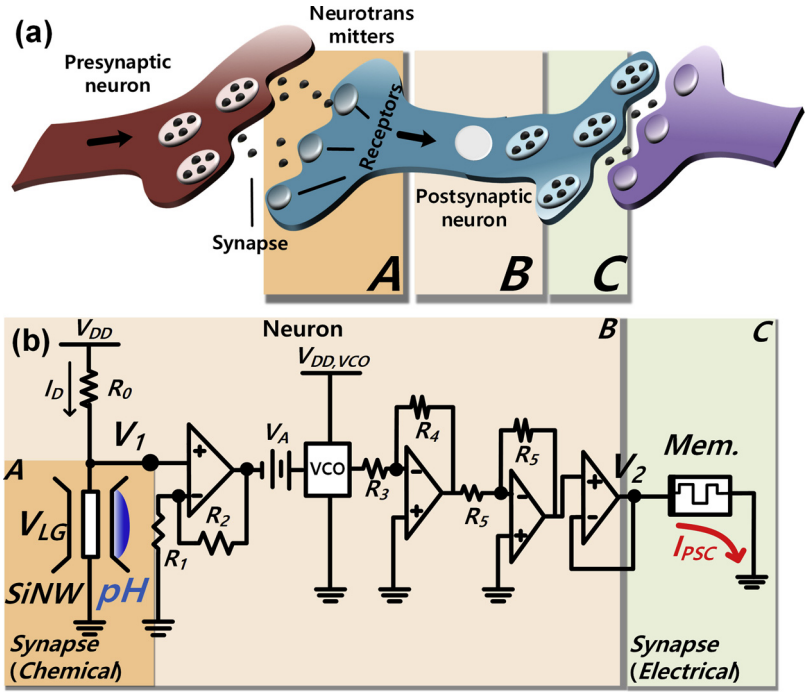


**Fig. 1.** (a) Biological synapse and neuron. (b) an Artificial synapse and a neuron.

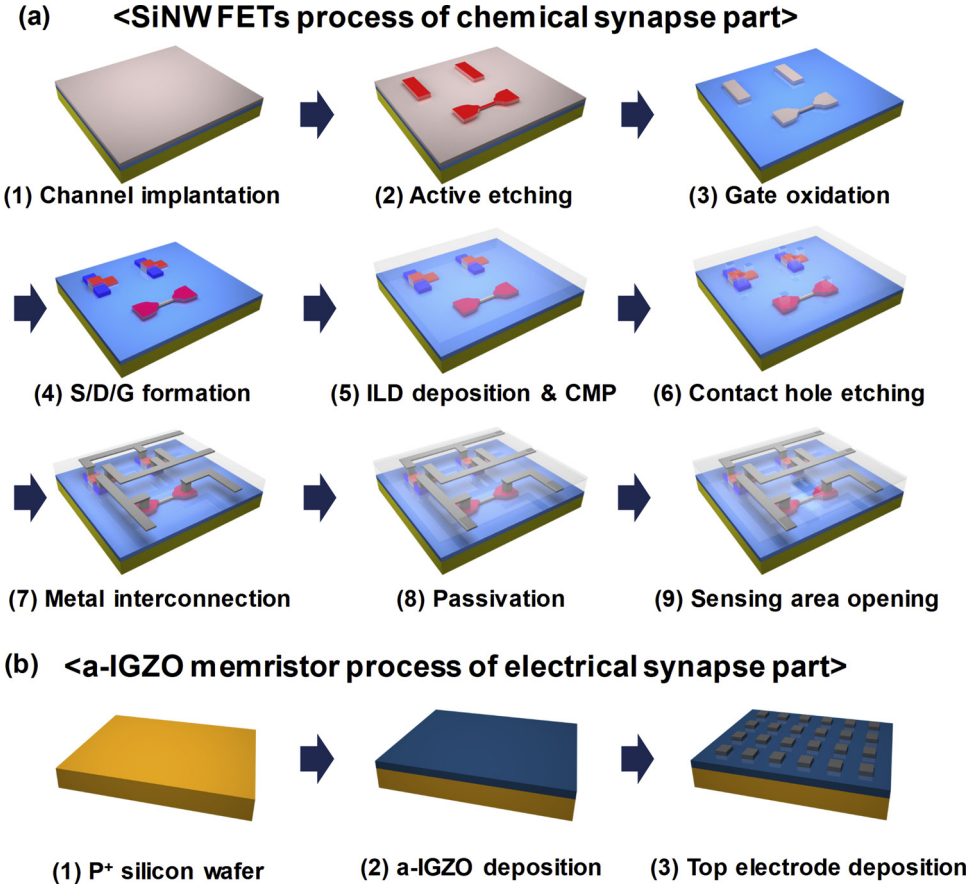


**Fig. 2.** Fabrication process of the (a) SiNW ISFET integrated with MOSFET and (b) a-IGZO memristor.

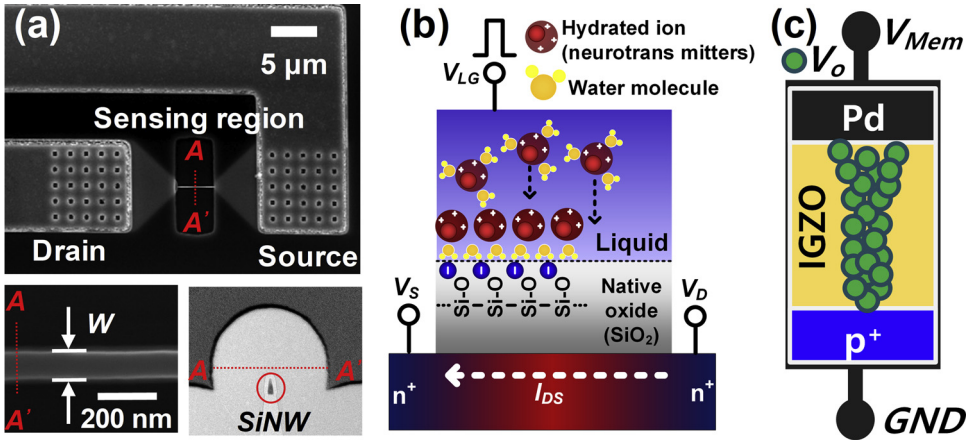


**Fig. 3.** (a) Top-view SEM and TEM image of the fabricated SiNW FETs. Schematic illustrations of (b) the SiNW ISFET playing the role of a chemical synapse and (c) a-IGZO memristor playing the role of an electrical synapse.

shown in Fig. 3(a). The SiNW ISFET and a-IGZO memristor are also schematically illustrated in Fig. 3(b) and (c), respectively.

## 3. Results and discussion

### 3.1. SiNW ISFETs as the chemical function of chemical synapses

To obtain a surface with an amine ($-NH_2$), the fabricated devices were functionalized using 3-aminopropyl-triethoxysilane (APTES) after an alloying process was conducted. By using 0.1 M potassium phosphate buffers (pH 5–9) for pH solutions, we eliminated the possible side effects caused by alkali metal ions by maintaining a constant concentration of alkali metal ions [9]. Therefore, our SiNWs could selectively respond to the presence of hydrogen ions. The fabricated SiNW ISFETs were characterized using a semiconductor parameter analyzer (4156C, Keysight) at room temperature under dark and ambient air conditions. The Ag/AgCl reference electrode was used as the liquid gate. The measured drain current ($I_D$)–liquid gate voltage ($V_{LG}$) curves under 2 V drain voltage ($V_D$) of the n-type and p-type SiNW ISFETs are shown in Fig. 4(a). The extracted threshold voltage ($V_T$) (n-type = 0.35 V, p-type = −0.25 V) was defined as the value of $V_{LG}$ at an $I_D$ of 10 nA. The SiNW ISFETs were successfully integrated into the CMOS circuits using a combination of a top-down approach and CMOS-compatible back-end process. The measured output characteristics of the SiNW ISFETs under various $V_{LG}$ values ($V_{LG}$ = 0.5–2 V with the step of 0.5 V) indicated that the SiNW ISFETs were operating under a saturated condition, as shown in Fig. 4(b). The transfer characteristics of the n-type SiNW ISFETs at the five studied pH values are shown in Fig. 4(c). At a low pH, the $-NH_2$ group was protonated to $-NH_3$, resulting in a greater positive potential. In contrast, at a high pH, the

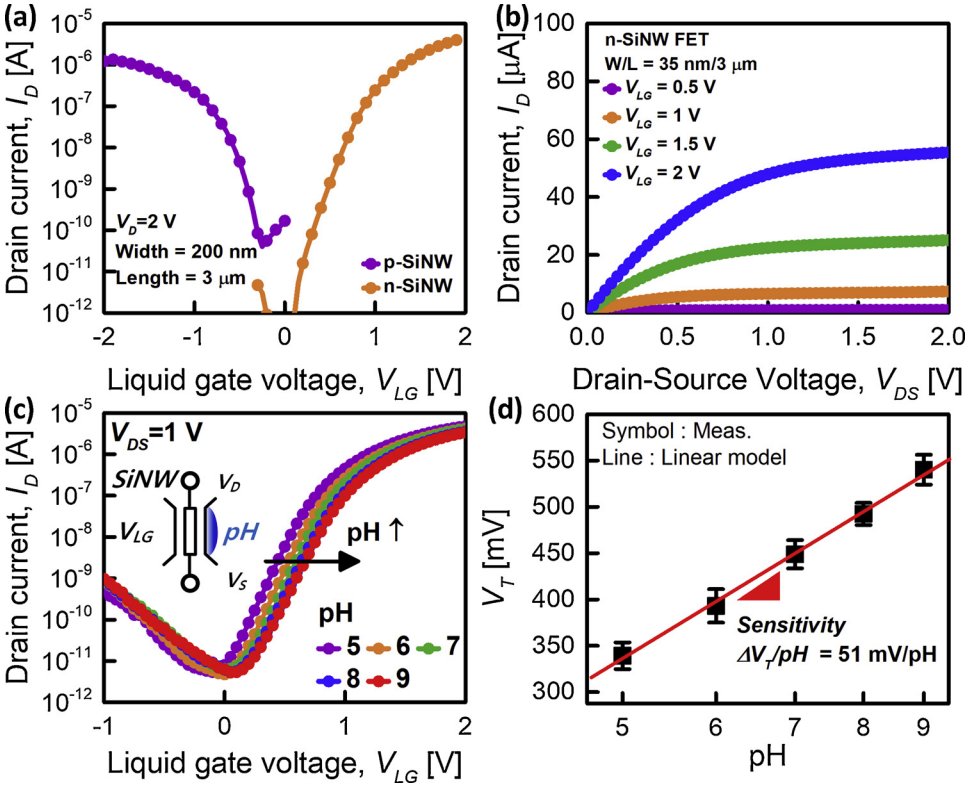


**Fig. 4.** (a) Drain current ($I_D$)–liquid gate voltage ($V_{LG}$) curves of n-channel and p-channel SiNW ISFETs and (b) $I_D$–$V_{DS}$ curves of n-channel SiNW ISFET under various $V_{LG}$ values. (c) The transfer characteristic and (d) $V_T$s according to the pH of n-type SiNW ISFETs ($V_T$ extracted using the constant current method at 10 nA).

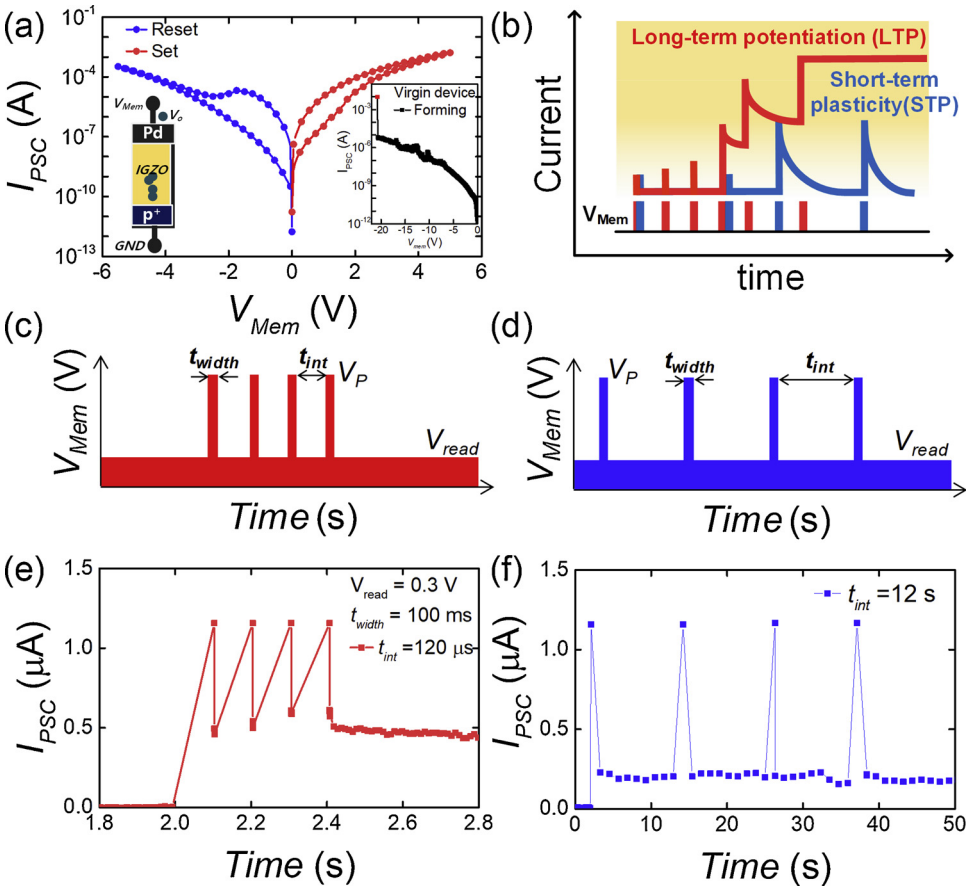


**Fig. 5.** Resistive switching characteristics of the a-IGZO memristor. (a) Current–voltage (*I–V*) curves of the a-IGZO memristor devices. The red and blue circles correspond to the set and reset characteristics, respectively. The inset of (a) shows a schematic illustration of an a-IGZO memristor device and forming characteristic. (b) Schematic image of the LTP and STP characteristic as a function of the voltage applied to the a-IGZO memristor ($V_{Mem}(t)$). Schematic illustrations of $V_{Mem}(t)$ pulses in (c) LTP and (d) STP conditions. Used pulse parameters are as follows: programing pulse amplitude $V_P = 4.5$ V, read pulse amplitude $V_{read} = 0.3$ V, duration of programing pulse train $t_{width} = 100$ ms, and interval between consecutive programing pulse trains $t_{int} = 120$ μs (LTP) and $t_{int} = 12$ s (STP), respectively. Measured $I_{PSC}$ of the a-IGZO memristor under (e) LTP and (f) STP conditions (For interpretation of the references to colour in this figure legend, the reader is referred to the web version of this article).

−SiOH group was deprotonated to −SiO−, resulting in a greater negative potential. The surface potential at the $SiO_2$/SiNW interface was thus confirmed to be well-modulated by pH values. The average shift of $V_T$ ($\Delta V_T$) by pH was 51 mV/pH, as shown in Fig. 4(d), which is similar to the Nernst limit (59 mV/pH) [16]. This process acts as a chemical function in chemical synapses, in which an action potential is generated after the neurotransmitters selectively bind to a receptor [5].

### 3.2. a-IGZO memristors as the part of synaptic plasticity

The bipolar resistive switching (RS) characteristic is observed in the a-IGZO memristor as seen in the current–voltage ($I_{PSC}$–$V_{Mem}$) curves in Fig. 5(a), where the postsynaptic current ($I_{PSC}$) and the voltage applied to the top electrode under the bottom electrode connected to GND ($V_{Mem}$) are defined as denoted in the left-inset of Fig. 5(a). In the right-side inset illustration of Fig. 5(a), the current of the virgin device is very low because of the detection limit of the electrical measurement system and the dielectric state. When the forming voltage of approximately −20 V is applied as $V_{Mem}$ with a compliance current of 0.01 A, the current radically flows, and the device is set to a low-resistance state (LRS). After the forming process, the stable RS between the LRS and high resistance state (HRS) is observed with $V_{RESET} = -5.5$ V (the voltage at which the LRS changes abruptly into HRS) and $V_{SET} = +5$ V (the voltage at which the HRS changes abruptly into LRS). The mechanism of the memristive behavior of a-IGZO memristors is known as the gradual growth/rupture of the conductive filament (CF) resulting from oxygen vacancies ($V_O$s) and the re-dox reaction between the resistive switching layer and metal electrodes [10–12,17]. The CF composed of the positively ionized oxygen vacancies ($V_O^{2+}$s) gradually grows and $I_{PSC}$ increases under a consecutive pulse, assigning a positive voltage with appropriate amplitude, i.e., potentiation. Meanwhile, the CF gradually ruptures and $I_{PSC}$ decreases under a consecutive pulse, assigning a negative voltage with appropriate amplitude, i.e., depression. Thus, the gradual modulation of CF using the consecutive $V_{Mem}$ pulse can emulate the LTP and STP in synapses. The characteristics of synaptic plasticity depending on the type of $V_{Mem}(t)$ pulse train is schematically illustrated in Fig. 5(b). When the potentiation pulse is applied more frequently, $I_{PSC}$ gradually increases and remains high for a long time even if the pulse is removed. That is, the synaptic strength is maintained in the enhanced state (LTP). On the other hand, as the potentiation pulse becomes less frequent, $I_{PSC}$ does not maintain the increased state and returns to the initial current. In other words, the synapse loses its strengthened state (STP). These synaptic plasticity phenomena are clearly observed in our devices, as depicted in Fig. 5(c)–(f). Schematic illustrations of $V_{Mem}(t)$ pulses are also shown for the LTP [Fig. 5(c)] and STP conditions [Fig. 5(d)]. The applied pulse parameters are as follows: potentiation pulse amplitude $V_P = 4.5$ V (the $V_P$ value is slightly lower than $V_{SET} = 5$ V because the gradual RS is required in the case of memristive operation), read pulse amplitude $V_{read} = 0.3$ V, duration of the programing pulse train $t_{width} = 100$ ms, and the interval between consecutive programing pulse trains $t_{int} = 120$ μs (LTP) and $t_{int} = 12$ s (STP), respectively. It is found that the $t_{int}$-dependence of the measured $I_{PSC}$ shows stable LTP [Fig. 5(e)] and STP characteristics [Fig. 5(f)]. The LTP current does not return to its original state as shown Fig. 5(e), which means that the short interval time is sufficient for the CF to form with a permanent configuration because of sufficient $V_O^{2+}$s generation. Meanwhile, the STP current quickly returns to the initial state, as shown in Fig. 5(f), indicating that the long interval time between pulses causes rapid decay of the CF resulting from the removal of $V_O^{2+}$s. Therefore, the memristive behavior and synaptic responses are in agreement with the plasticity of biological synapses, showing that the synaptic weight is dynamically updated and time-dependently memorized by repeated stimulation.

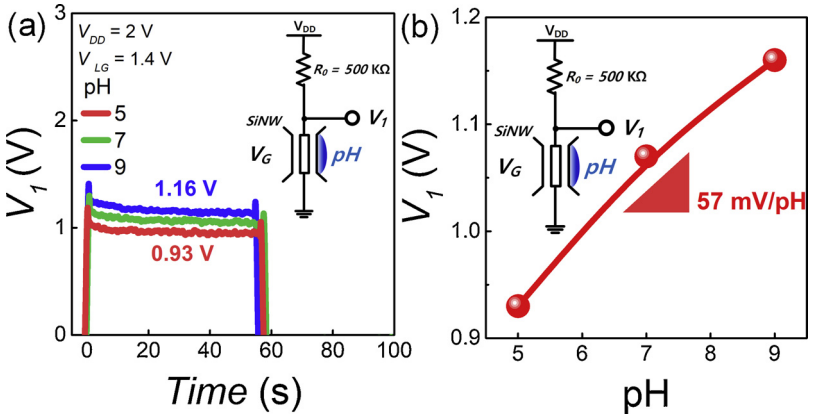


**Fig. 6.** (a) Measured time-varying $V_1$ and (b) pH-dependent $V_1$ (Inset: The chemical synapse based on the SiNW ISFET).

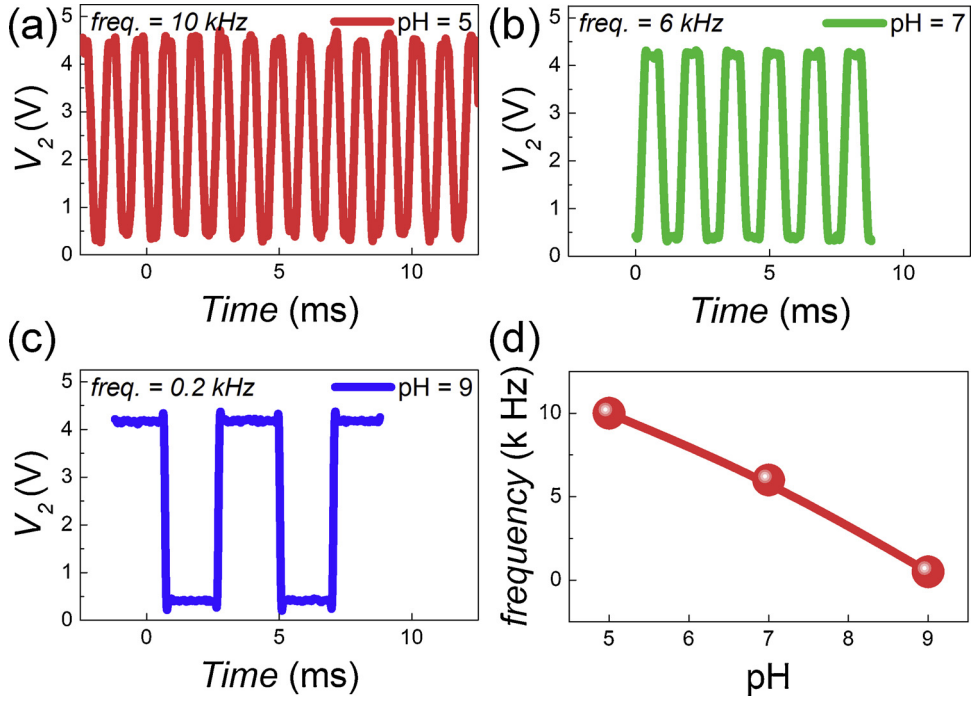


**Fig. 7.** Measured $V_2$ when (a) pH = 5, (b) pH = 7, and (c) pH = 9. (d) The pH-dependent frequency of $V_2$ (Inset: Schematic of the VCO).

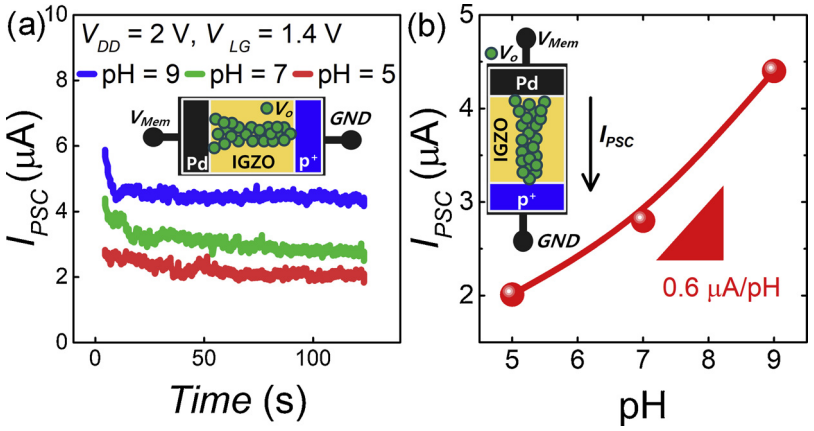


**Fig. 8.** (a) Measured pH-dependent $I_{PSC}$-time characteristic when $V_{read}$ = 0.5 V. (b) pH-dependent $I_{PSC}$ (Inset: Schematic of the a-IGZO memristor as the electrical synapse).

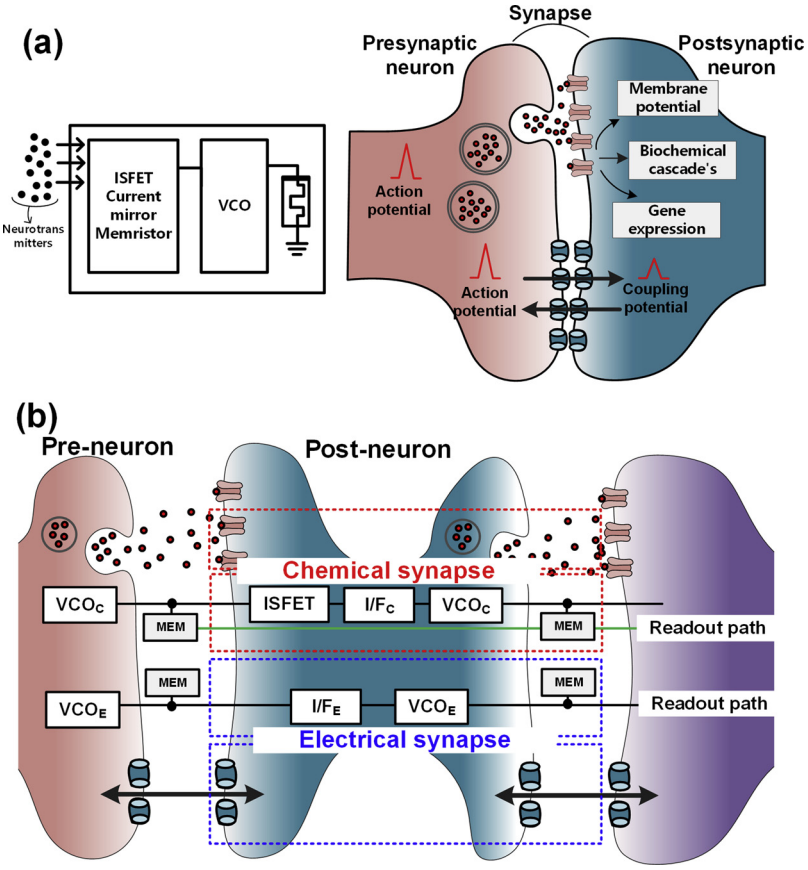


**Fig. 9.** (a) The schematic of the mixed synapse of chemical and electrical synapses in a single platform. (b) The proposed platform implementing and emulating the electrical and chemical synapses by using the ISFET, VCO, and memristor. The signal propagation and memorization/update of synaptic strength are considered separately.

### *3.3. Artificial synapse and neuron circuit conducting the electrical-chemical-electrical signal conversion in chemical synapses*

To implement the brain-inspired circuit in a single platform, the hydrogen ion concentration-modulated current ($I_{DS}$) of SiNW ISFET, which plays the role of a chemical function of chemical synapse as illustrated in part A of Fig. 1(b), should be converted to the output voltage ($V_1$) as shown Fig. 6 according to the following equations:

$$V_1 = V_{DD} - I_{DS} \cdot R_0, \tag{1}$$

$$V_1 = V_{DD} - \mu \cdot C_{ox} \cdot \frac{W}{2L} \cdot \{V_{LG} - V_T(pH)\}^2 \cdot R_0, \tag{2}$$

where $V_1$ is the output voltage, $V_{DD}$ is the supply voltage, $I_{DS}$ is the drain current of the SiNW ISFET, $R_0$ is the output resistance, μ is the electron mobility, $C_{ox}$ is the gate oxide capacitance per unit area, $W$ is the width of the SiNW ISFET, $L$ is the length of the SiNW ISFET, $V_{LG}$ is the liquid gate voltage, and $V_T$ is the threshold voltage of the SiNW ISFET. The value of $R_0$ is selected as 500 kΩ by considering the relationship between the driving ability of the SiNW ISFET and the voltage for operating the next stage. At a pH of 5 and 9, $V_1$ is 0.93 and 1.16 V, respectively. At pH = 5, the $V_T$ becomes lowered, allowing an increase in $I_{DS}$. The pH sensitivity of the device ($V_1$/pH) is 0.57 mV/pH. It indicates the ability of the device to selectively convert the concentration of biomolecules, e.g., hydrogen ions and/or neurotransmitters, into an electrical signal $V_1$ and mimic the chemical-electrical signal conversion of chemical synapses. The results suggest that the developed ISFET can transform the concentration of neurotransmitter agents into the output voltage $V_1$ of the neuron circuit with the functionalization of their specific-binding receptors.

Artificial neuron models have been used by the integrate-and-fire, Hodgkin-Huxley, Izhikevich, Mihalas-Niebur, and other models [18]. In our case, for hardware simplicity, a VCO (LTC6990, Linear Technology) is chosen as a neuron, as illustrated in part B of Fig. 1(b). This is so because from the standpoint of memristors, the voltage oscillator with an oscillation frequency modulated by the $V_1$ depending on the concentration of target biomolecules can play the same role as the $V_{Mem}$ pulse train shown in Fig. 5(b). Moreover, the VCO is a well-known stable oscillator and is widely used in the field of electronics where frequency and phase modulation is indispensable for a phase-locked loop, delay-locked loop, and clock data recovery. In addition, as shown in part B of Fig. 1(b), a few operational amplifiers (OP497) and resistors were used to optimize each operating point voltage. The values of resistors $R_1$, $R_2$, $R_3$, $R_4$, and $R_5$ were 2, 5, 12, 5, and 12 kΩ, respectively. Frequency of the output voltage ($V_2$) of the employed VCO is then modulated by the pH-dependent $V_1$, as shown in Fig. 7. As pH decreases from 9 to 7 and then again to 5, the frequency of $V_2$ also decreases from 10 to 6 and further to 0.2 kHz, respectively, indicating emulation of the train of output spikes out of postsynaptic neurons, i.e., the group of dendrite-cell body-axons, including the integration and firing functions.

Finally, the $I_{PSC}$ is programmed to the a-IGZO memristor for modulating the strength of synaptic connectivity, as illustrated in part C of Fig. 1(b). Fig. 8(a) shows the measured pH-dependent $I_{PSC}$ when a pulse train is applied. At pH = 5, the $I_{PSC}$ level is low (HRS state) because the short duration pulses cause the STP. At pH = 9, the level of read $I_{PSC}$ is high (LRS state) because the long duration pulses cause the LTP. The sensitivity of $I_{PSC}$ to the pH value, i.e., the sensitivity of the strength of the synaptic connection to the concentration of the neurotransmitter, was 0.6 μA/pH, as shown in Fig. 8(b).

These experimental results clearly show the chemical-electrical signal conversion of chemical synapses in a single platform, as summarized in Fig. 9(a), indicating that brain-inspired models and algorithms can be potentially studied considering the relationship between the chemical and electrical synaptic functions of the human brain or nervous system. In turn, the proposed platform can be easily expanded to the implementation and emulation of electrical synapses only if the ISFET part is excluded and the VCO is substituted by a much faster part

along with the addition of a bidirectional path (the signal propagation in electrical synapses is much faster than that in chemical synapses), as depicted in Fig. 9(b). Furthermore, in the proposed platform, the path through which neuro-signals propagate and the path where synaptic strengths are stored and dynamically updated can be taken into account separately only if the readout path for reading the status of memristors, i.e., synaptic strength, is added as shown in Fig. 9(b).

## 4. Conclusion

In this study, the electrical-chemical signal conversion in chemical synapses, signal propagation via neurons, and the resultant plasticity of synaptic strength were demonstrated in a single platform by combining the pH sensing and LTP/STP capability of an ISFET and IGZO memristor using a VCO as the link between two devices. The concentration of ions was successfully transformed via a simple neuron circuit block into modulation of the post-synapse current of a memristor. These circuits were not integrated and did not directly detect neurotransmitters; further, they did not use sophisticated neuron circuits. However, the proposed artificial synapse and neuron simultaneously simulated the chemical and electrical behaviors of synapses.

Furthermore, our results indicate the feasibility of discriminating the chemical synapse from the electrical synapse and considering the path of neuro-signal propagation and the path of memorization/update of synaptic strength separately. The proposed platform composed of artificial synapses and neurons is thus potentially useful for emulating the human brain more realistically from the perspective of brain-inspired computing and for creating a new computational platform to explore the secrets of the ultrahigh energy-efficiency, adaptive learning, and disease mechanism of the human brain.

## Acknowledgments

This work was supported by the NRF funded by the Korean government under Grant 2016R1A5A1012966, 2016M3A7B4909668, 2017R1A2B4006982, and in part by ETRI grant funded by the Korean government (18ZB1800). The CAD software was supported by SYNOPSYS and IDEC.

## References

[1] T. Fujita, The smaller occipital nerve, its topographic relation to the trapezius-sternocleidomastoideus muscle system, Okajimas Folia Anat. Jpn. 33 (1959) 217–224, https://doi.org/10.2535/ofaj1936.33.4_217.
[2] S.A. McKee, Reflections on the memory wall, Proc. First Conf. Comput. Front. Comput. Front. - CF'04 (2004) 162, https://doi.org/10.1145/977091.977115.
[3] C.-S. Poon, K. Zhou, Neuromorphic silicon neurons and large-scale neural networks: challenges and opportunities, Front. Neurosci. 5 (2011) 2009–2011, https://doi.org/10.3389/fnins.2011.00108.
[4] S. Yu, Neuro-inspired Computing Using Resistive Synaptic Devices, Springer International Publishing, Cham, 2017, https://doi.org/10.1007/978-3-319-54313-0.
[5] S. Thanapitak, C. Toumazou, A bionics chemical synapse, IEEE Trans. Biomed. Circuits Syst. 7 (2013) 296–306, https://doi.org/10.1109/TBCAS.2012.2202494.
[6] M. Bear, B. Connors, M. Paradiso, Neuroscience: Exploring the brain, 4th ed., Wolters Kluwer, 2016.
[7] A.E. Pereda, Electrical synapses and their functional interactions with chemical synapses, Nat. Rev. Neurosci. 15 (2014) 250–263, https://doi.org/10.1038/nrn3708.
[8] T. Ohno, T. Hasegawa, T. Tsuruoka, K. Terabe, J.K. Gimzewski, M. Aono, Short-term plasticity and long-term potentiation mimicked in single inorganic synapses, Nat. Mater. 10 (2011) 591–595, https://doi.org/10.1038/nmat3054.
[9] J. Lee, J.-M. Lee, J.H. Lee, M. Uhm, W.H. Lee, S. Hwang, I.-Y. Chung, B.-G. Park, D.M. Kim, Y.-J. Jeong, D.H. Kim, SiNW-CMOS hybrid common-source amplifier as a voltage-readout hydrogen ion sensor, IEEE Electron Device Lett. 34 (2013) 135–137, https://doi.org/10.1109/LED.2012.2226136.
[10] S. Kim, J. Kim, J. Jang, H.-S. Mo, D.M. Kim, S.-J. Choi, B.-G. Park, D.H. Kim, J. Park, Sampling time and pH-dependences of silicon nanowire ion-sensitive field-effect transistor-based biosensors, J. Nanosci. Nanotechnol. 17 (2017) 3257–3260, https://doi.org/10.1166/jnn.2017.14038.
[11] D.W. Kwon, S. Kim, R. Lee, H.-S. Mo, D.H. Kim, B.-G. Park, Macro modeling of ion sensitive field effect transistor with current drift, Sens. Actuators B Chem. 249 (2017) 564–570, https://doi.org/10.1016/j.snb.2017.03.110.
[12] Z.Q. Wang, H.Y. Xu, X.H. Li, H. Yu, Y.C. Liu, X.J. Zhu, Synaptic learning and memory functions achieved using oxygen ion migration/diffusion in an amorphous InGaZnO memristor, Adv. Funct. Mater. 22 (2012) 2759–2765, https://doi.org/10.1002/adfm.201103148.
[13] S. Kim, C. Du, P. Sheridan, W. Ma, S. Choi, W.D. Lu, Experimental demonstration of a second-order memristor and its ability to biorealistically implement synaptic plasticity, Nano Lett. 15 (2015) 2203–2211, https://doi.org/10.1021/acs.nanolett.5b00697.
[14] J.T. Jang, D. Ko, G. Ahn, H.R. Yu, H. Jung, Y.S. Kim, C. Yoon, S. Lee, B.H. Park, S.-J. Choi, D.M. Kim, D.H. Kim, Effect of oxygen content of the LaAlO 3 layer on the synaptic behavior of Pt/LaAlO 3/Nb-doped SrTiO 3 memristors for neuromorphic applications, Solid. Electron. 140 (2018) 139–143, https://doi.org/10.1016/j.sse.2017.10.032.
[15] W. Hu, L. Zou, X. Chen, N. Qin, S. Li, D. Bao, Highly uniform resistive switching properties of amorphous InGaZnO thin films prepared by a low temperature photochemical solution deposition method, ACS appl. Mater. Interfaces 6 (2014) 5012–5017, https://doi.org/10.1021/am500048y.
[16] M.J. Madou, S.R. Morrison, Chemical Sensing with Solid State Devices, Elsevier, 1989, https://doi.org/10.1016/C2009-0-22258-6.
[17] R. Jiang, P. Ma, Z. Han, X. Du, Habituation/fatigue behavior of a synapse memristor based on IGZO–HfO2 thin film, Sci. Rep. 7 (2017) 9354, https://doi.org/10.1038/s41598-017-09762-5.
[18] B. Datta Sahoo, Ring oscillator based sub-1V leaky integrate-and-fire neuron circuit, 2017 IEEE Int. Symp. Circuits Syst., IEEE (2017) 1–4, https://doi.org/10.1109/ISCAS.2017.8050980.

**Sungju Choi** received the B.S. and M.S. degrees in electrical engineering from Kookmin University, Seoul, South Korea, in 2016, where he is currently pursuing the Ph.D. degree with the Department of Electrical Engineering.

**Seohyeon Kim** received the B.S. and M.S. degrees in electrical engineering from Kookmin University, Seoul, South Korea, in 2018, where he is currently pursuing the Ph.D. degree with the Department of Electrical Engineering.

**Jungkyu Jang** received the B.S. and M.S. degrees in electrical engineering from Kookmin University, Seoul, South Korea, in 2018, where he is currently pursuing the Ph.D. degree with the Department of Electrical Engineering.

**Geumho Ahn** received the B.S. degree in electrical engineering from Kookmin University, Seoul, South Korea, in 2017, where he is currently pursuing the M.S. degree with the Department of Electrical Engineering.

**Jun Tae** Jang received the B.S. and M.S. degrees in electrical engineering from Kookmin University, Seoul, South Korea, in 2016, where he is currently pursuing the Ph.D. degree with the Department of Electrical Engineering.

**Jinsu Yoon** received the B.S. and M.S. degrees in electrical engineering from Kookmin University, Seoul, South Korea, in 2016, where he is currently pursuing the Ph.D. degree with the Department of Electrical Engineering.

**Tae Jung Park** received the B.S. and M.S. degrees from Chungnam National University, Daejeon, Korea, in 1998 and 2000, respectively, and the Ph.D. degree from the Korea Advanced Institute of Science and Technology, Daejeon, in 2008.

**Byung-Gook Park** received the B.S. and M.S. degrees in electronic engineering from Seoul National University (SNU), Seoul, Korea, in 1982 and 1984, respectively, and the Ph.D. degree in electrical engineering from Stanford University, Stanford, CA,USA, in 1990. He joined the School of Electrical Engineering, SNU, in 1994, as an Assis-tant Professor, where he is currently a Professor. He holds more than 100 Korean and U.S. patents

**Sung-Jin Choi** received the M.S. and Ph.D. degrees in electrical engineering from the Korea Advanced Institute of Science and Technology, Daejeon, South Korea, in 2012. He is currently an Assistant Professor with the School of Electrical Engineering, Kookmin University, Seoul, South Korea.

**Dong Myong Kim** received the B.S. and M.S. degrees in electronics engineering from Seoul National University, Seoul, South Korea, in 1986 and 1988, respectively, and the Ph.D. degree in electrical engineering from the University of Minnesota Twin Cities, Minneapolis, MN, USA, in 1993. He is currently a Professor with the School of Electrical Engineering, Kookmin University, Seoul.

**Seung Min Lee** received the B.S. degree in electronics engineering from Sogang University, Seoul, Korea, in 2005, and the M.S. and Ph.D. degrees in interdisciplinary program for bioengineering from Seoul National University, Seoul, Korea, in 2007 and 2012, respectively. He was a research professor at Korea University, Seoul, Korea, from 2012 to 2014, and worked as a postdoctoral researcher at University of Illinois at Urbana/Champaign, Champaign, IL, USA, from 2014 to 2017. He is currently an assistant professor in Kookmin University, Seoul, Korea. His research interests include active microelectrodes, new electronic materials, and electronic devices for biomedical engineering.

**Eun Young Kim** received the B.S., M.S. degrees in Biology from Yonsei University, Seoul,

Korea and Ph.D. degree in Neuroscience from Ajou University, Suwon, Korea in 1992, 1994, and 2000, respectively. She is currently a Professor of Department of Brain Science at Ajou University, School of Medicine, Suwon, Korea. Her research interests include molecular mechanisms of circadian clock, role of circadian clock in normal brain function and neurodegenerative diseases, and human disease modeling using Drosophila.

**Hyun-Sun Mo** received the B.S., M.S., and Ph.D degrees in Electronic Engineering from Kookmin University, Seoul, Korea, in 1993 and 2011, and 2014, respectively. In1993, she joined Samsung Electronics Semiconductor Division of the development of the low power and high-speed SRAM and Flash memory circuits. Her research interests include the design of analog circuits, power-management ICs, and the next-generation memories.

**Dae Hwan Kim** received the B.S., M.S., and Ph.D. degrees in electrical engineering from Seoul National University, Seoul, Korea, in 1996, 1998, and 2002, respectively. He is currently a Professor with the School of Electrical Engineering, Kookmin University, Seoul, Korea. His current research interests include nano CMOS, oxide and organic thin-film transistors, biosensors, and neuromorphic devices.